



1 **Rapid transition in winter aerosol composition in Beijing from 2014 to** 2 **2017: response to clean air actions**

3 Haiyan Li^{1,a}, Jing Cheng², Qiang Zhang², Bo Zheng¹, Yuxuan Zhang², Guangjie Zheng¹, Kebin He^{1,3}

4 ¹ State Key Joint Laboratory of Environment Simulation and Pollution Control, School of Environment, Tsinghua University,
5 Beijing 100084, China

6 ² Ministry of Education Key Laboratory for Earth System Modeling, Department of Earth System Science, Tsinghua University,
7 Beijing 100084, China

8 ³ State Environmental Protection Key Laboratory of Sources and Control of Air Pollution Complex, Tsinghua University, Beijing
9 100084, China

10 ^apresent address: Institute for Atmospheric and Earth System Research/Physics, Faculty of Science, University of Helsinki, 00014
11 Helsinki, Finland

12 *Correspondence:* Qiang Zhang (qiangzhang@tsinghua.edu.cn)

13 **Abstract.** The clean air actions implemented by the Chinese government in 2013 have led to significantly improved air quality in
14 Beijing. In this work, we combined the in-situ measurements of the chemical components of submicron particles (PM₁) in Beijing
15 during the winters of 2014 and 2017 and a regional chemical transport model to investigate the impact of clean air actions on
16 aerosol chemistry and quantify the relative contributions of anthropogenic emissions, meteorological conditions, and regional
17 transport to the changes in aerosol chemical composition from 2014 to 2017. We found that the average PM₁ concentration in
18 winter in Beijing decreased by 49.5% from 2014 to 2017 (from 66.2 μg m⁻³ to 33.4 μg m⁻³). Sulfate exhibited a much larger decline
19 than nitrate and ammonium, which led to a rapid transition from sulfate-driven to nitrate-driven aerosol pollution during the
20 wintertime. Organic aerosol (OA), especially coal combustion OA, and black carbon also showed large decreasing rates, indicating
21 the effective emission control of coal combustion and biomass burning. The decreased sulfate contribution and increased nitrate
22 fraction were highly consistent with the much faster emission reductions in sulfur dioxide (SO₂) due to phasing out coal in Beijing
23 compared to reduction in nitrogen oxides emissions estimated by bottom-up inventory. The chemical transport model simulations
24 with these emission estimates reproduced the relative changes in aerosol composition and suggested that the reduced emissions in
25 Beijing and its surrounding regions played a dominant role. The variations in meteorological conditions and regional transport
26 contributed much less to the changes in aerosol concentration and its chemical composition during 2014-2017 compared to the
27 decreasing emissions. Finally, we observed that changes in precursor emissions also altered the aerosol formation mechanisms.
28 The decreased SO₂ emissions suppressed the rapid formation of secondary sulfate through heterogeneous reactions. The observed
29 explosive growth of sulfate at a relative humidity (RH) greater than 50% in 2014 was delayed to a higher RH of 70% in 2017.
30 Thermodynamic simulations showed that the decreased sulfate and nitrate concentrations have lowered the aerosol water content,
31 particle acidity, and ammonium particle fraction. The results in this study demonstrated the response of aerosol chemistry to the
32 stringent clean air actions and identified that the anthropogenic emission reductions are a major driver, which could help to further
33 guide air pollution control strategies in China.

34 **1 Introduction**

35 Beijing, the capital of China, is one of the most heavily polluted cities in the world (Lelieveld et al., 2015), and it frequently
36 experiences severe and persistent haze pollution episodes in winter (Guo et al., 2014). For example, in January 2013, the daily
37 concentration of ambient particles with an aerodynamic diameter less than 2.5 μm (PM_{2.5}) reached a record high of 569 μg m⁻³ in
38 Beijing (Ferreri et al., 2018), which was over 20 times higher than the World Health Organization standard (25 μg m⁻³ for daily



39 average $PM_{2.5}$). As a complex mixture of many different components, ambient aerosols have a range of chemical compositions and
40 originate from various emission sources and formation processes in the atmosphere (Seinfeld and Pandis, 2012). The adverse
41 effects of aerosols on visibility (Pui et al., 2014), climate (IPCC, 2013), and human health (Pope et al., 2009) are intrinsically
42 related to the chemical composition of particles.

43 To tackle severe aerosol pollution, the Chinese State Council implemented the Air Pollution Prevention and Control Action Plan
44 (denoted as clean air actions) in September 2013, which is the most stringent pollution mitigation policy ever in China. As a
45 consequence, China's anthropogenic emissions have declined by 59% for SO_2 , 21% for NO_x , 32% for organic carbon (OC), and
46 28% for black carbon (BC) during 2013-2017 (Zheng et al., 2018). The annual average $PM_{2.5}$ concentration in Beijing decreased
47 by 35.6% from 2013 to 2017, reaching $58 \mu g m^{-3}$ in 2017. Combining the bottom-up emission inventory and chemical transport
48 model simulations, our recent study (Cheng et al., 2019) quantified the relative contributions of meteorological conditions,
49 emission reductions from surrounding regions, and emission reductions from local sources to the decrease in $PM_{2.5}$ concentration
50 in Beijing during 2013-2017. While changes in meteorological conditions partially explained air quality improvement in Beijing
51 in 2017, local and regional emission controls played major roles. In addition, the aerosol chemical composition is expected to
52 change correspondingly due to the rapid reductions in precursor emissions, which is not well understood yet because the chemical
53 components of $PM_{2.5}$ are not measured by China's monitoring network. A few studies have examined the change in aerosol
54 composition in Beijing after 2013, including a semicontinuous measurement of carbonaceous aerosols during 2013-2018 (Ji et al.,
55 2019) and an aerosol mass spectrometry study comparing aerosol composition and size distribution between 2014 and 2016 (Xu
56 et al., 2018). However, neither performed a comprehensive assessment of all the main factors affecting aerosol concentration and
57 its composition. A deep understanding of how the aerosol composition has changed since the clean air actions were activated and
58 the possible linkage between them is urgently needed.

59 The chemical composition of $PM_{2.5}$ is mainly affected by three factors: precursor emissions, meteorological conditions, and
60 regional transport patterns. Emissions are typically the main driver of aerosol composition changes. During 2005-2012, the sulfate
61 concentration in China decreased, while the nitrate concentration increased, which was caused by the considerable reduction in
62 SO_2 emissions but limited control of NO_x (Geng et al., 2017). Based on the measurements of organic aerosol (OA) composition in
63 Beijing, a larger decrease in secondary OA than primary OA was found during the 2014 Asia-Pacific Economic Cooperation
64 summit due to the strict emission controls (Sun et al., 2016). Meteorological conditions affect aerosol composition by changing
65 emissions, chemical reactions, and transport and deposition processes (Mu and Liao, 2014). For example, increases in relative
66 humidity (RH) enhance the secondary formation of sulfate through heterogeneous reactions (Zheng et al., 2015; Cheng et al., 2016),
67 and decreases in temperature favor particulate nitrate formation by facilitating gas-to-particle partitioning (Pye et al., 2009; Li et
68 al., 2018). With chemical transport model simulations in China for the years 2004-2012, Mu and Liao (2014) demonstrated that
69 due to the large variations in meteorological parameters in North China, all aerosol species showed large corresponding interannual
70 variations. Furthermore, aerosol characteristics in Beijing are influenced by regional transport from adjacent polluted regions.
71 Polluted air masses from the southern regions contributed more secondary inorganic aerosols (SIAs) than primary aerosols in
72 Beijing (Zhang et al., 2014; Du et al., 2018).

73 Following our previous work (Cheng et al., 2019), the main objective of this study is to investigate the impact of clean air actions
74 on changes in aerosol chemical composition from 2014 to 2017. With both the in-situ observations of aerosol species in Beijing
75 during the winters of 2014 and 2017 and model simulations for the corresponding periods, this work provides the opportunity for
76 a detailed evaluation of the underlying drivers. First, changes in aerosol characteristics are illustrated for inorganics and organics
77 by comparing aerosol measurements in 2014 and 2017. Then, the relative importance of different factors in varying aerosol
78 composition is assessed by combining direct observations and model simulations, including synoptic conditions, emission changes,



79 regional transport and formation mechanisms. Last, we show that the transition in aerosol characteristics influenced particle
80 properties, such as aerosol water content (AWC) and particle acidity, which in turn affects secondary aerosol formation.

81 **2 Experimental methods**

82 **2.1 Ambient sampling and instrumentation**

83 Online aerosol measurements were performed in urban Beijing during the winters of 2014 (from 6 December 2014 to 27 February
84 2015) and 2017 (from 11 December 2017 to 2 February 2018). The sampling site is located on the roof of a three-story building
85 on the campus of Tsinghua University (40.0° N, 116.3° E), which is surrounded by school and residential areas. No major industrial
86 sources are situated nearby. An Aerodyne Aerosol Chemical Speciation Monitor (ACSM) was deployed for the real-time chemical
87 observations of nonrefractory PM₁ (NR-PM₁), including organics, sulfate, nitrate, ammonium, and chloride. A detailed description
88 of the instrument can be found in Ng et al. (2011a). The mass concentration of BC in PM₁ was measured using a multiangle
89 absorption photometer (MAAP, model 5012; Petzold and Schönlinner, 2004). In addition, the total PM_{2.5} mass was simultaneously
90 recorded with a PM-712 monitor based on the β -ray absorption method (Kimoto Electric Co., Ltd., Japan). For gaseous species,
91 the mixing ratios of SO₂, NO_x, CO, and O₃ were monitored by a suite of commercial gas analyzers (Thermo Scientific). The
92 meteorological parameters, including temperature, RH, wind speed (WS), and wind direction (WD), were obtained from an
93 automatic meteorological observation instrument (MILOS520, VAISALA Inc., Finland).

94 **2.2 ACSM data analysis**

95 The ACSM data were analyzed using the standard analysis software within Igor Pro (WaveMetrics, Inc., Oregon USA). Default
96 relative ionization efficiencies (RIEs) were applied to organics (1.4), nitrate (1.1), and chloride (1.3), while the RIEs of ammonium
97 and sulfate were experimentally determined through calibrations with pure ammonium nitrate and ammonium sulfate, respectively.
98 A composition-dependent collection efficiency (CE) algorithm was used to account for the incomplete detection of aerosol particles
99 (Middlebrook et al., 2012). As shown in Fig. S1, the total measured PM₁ mass (NR-PM₁ plus BC) correlated well with the PM_{2.5}
100 obtained from PM-712 ($r^2 = 0.80$ and 0.87 for 2014 and 2017, respectively). On average, PM₁ accounted for 68% and 80% of the
101 total PM_{2.5} in Beijing during the winters of 2014 and 2017.

102 The ACSM provides unit-mass-resolution mass spectra of submicron particles, facilitating source apportionment via factor analysis.
103 In this study, positive matrix factorization (PMF) was implemented to resolve OA into various sources using a multilinear engine
104 (ME-2; Paatero, 1999) via the SoFi toolkit (Source Finder; Canonaco et al., 2013). The a value approach allows for the introduction
105 of a priori factor profile or time series to reduce the rotational ambiguity and obtain a unique solution. The spectra and error
106 matrices of organics were pretreated based on the procedures given by Ulbrich et al. (2009) and Zhang et al. (2011). Ions up to m/z
107 120 were considered in this study given the interferences of the internal standard of naphthalene at m/z 127-129 and the low signal-
108 to-noise ratio of larger ions. For the winter of 2014, a reference hydrocarbon-like OA (HOA) profile from Ng et al. (2011b) was
109 introduced into the ME-2 analysis, varying a value from 0 to 1. After a detailed evaluation of the factor profiles, time series, diurnal
110 variations, and correlations with external tracers, an optimal solution with four factors was finally accepted, with an a value of 0.
111 Figure S2 shows the source apportionment results with three primary factors, i.e., HOA, coal combustion OA (CCOA), and biomass
112 burning OA (BBOA), and one secondary factor, oxygenated OA (OOA). For the 2017 dataset, the mass spectral profiles of HOA,
113 CCOA, and BBOA from the ME-2 analysis for 2014 were adopted to constrain the model performance. Similarly, a four-factor
114 solution with HOA, BBOA, CCOA, and OOA was selected for the winter of 2017, which allowed a better comparison of the OA
115 sources between 2014 and 2017.



116 2.3 WRF-CMAQ model

117 The Weather Research and Forecasting (WRF) model, version 3.8, and the Community Multiscale Air Quality (CMAQ) model,
118 version 5.1, were applied to evaluate the impact of meteorological changes, regional transport and emission variations on the PM_{2.5}
119 concentration in Beijing in winter. The simulated area was designed as three nested domains, and the innermost area covered
120 Beijing and its surrounding regions (including Tianjin, Hebei, Shanxi, Henan, Shandong and Inner Mongolia), with a horizontal
121 resolution of 4 km × 4 km. The simulated period basically followed the observation time, which covered October 2014 – February
122 2015 and October 2017 – February 2018. A one-month spin-up was applied in each simulation.

123 The WRF model is driven by the National Centers for Environmental Prediction Final Analysis (NCEP-FNL) reanalysis data,
124 which then provided the meteorological fields for the CMAQ model. We used CB05 and AERO6 as the gas and particulate matter
125 chemical mechanisms, respectively. The in-line windblown dust and photolytic rate calculation modules were also adopted to
126 improve the simulation. The chemical initial and boundary conditions originated from the interpolated outputs of the Goddard
127 Earth Observing System with chemistry (GEOS-Chem) model (Bay et al., 2001).

128 The anthropogenic emission inventory for Beijing was taken from the Beijing Municipal Environmental Monitoring Center
129 (BMEMC), which was documented and analyzed in Cheng et al. (2019), while the emission inventory outside Beijing was provided
130 by the Multi-resolution Emission Inventory for China (MEIC) (<http://www.meicmodel.org>; Zheng et al., 2018) and the MIX
131 emission inventory for the other Asian countries (M. Li et al., 2017). The biogenic emissions were obtained by the Model of
132 Emission of Gases and Aerosols from Nature (MEGAN v2.1); however, open biomass burning was not considered in this work.
133 Detailed model configurations and validations can be found in Cheng et al. (2019), and the simulated results well reproduced the
134 temporal and spatial distributions and variations in PM_{2.5} in Beijing and its surrounding areas. The average simulated PM_{2.5} in
135 Beijing decreased from 91.5 (winter of 2014) to 52.5 (winter of 2017) μg m⁻³, with a total decrease of 39 μg m⁻³, while the observed
136 PM_{2.5} varied from 81.9 to 40.6 μg m⁻³, decreasing by 41.3 μg m⁻³. The Pearson correlation coefficients (R) between the simulated
137 and observed PM_{2.5} in Beijing were 0.81 (winter of 2014) and 0.78 (winter of 2017).

138 We designed six simulation cases to investigate the impact of meteorological and emission variations. Two base cases were driven
139 by the actual emission inventory and meteorological conditions in the winter of 2014 (case A) and winter of 2017 (case B). Cases
140 C and D were designed to quantify the impact of meteorological changes; case C was simulated with the emissions in 2014 and
141 meteorological conditions of 2017, while case D used the 2017 emissions and 2014 meteorological conditions. Therefore, the
142 differences between A and C or between B and D show the influence of meteorological conditions, and the differences between A
143 and D or between B and C correspond to the contributions of emission variations. We used the averaged differences as the final
144 impacts. Cases E and F were developed to evaluate the effect of regional transport on PM_{2.5} variations in Beijing in the winter of
145 2014 (E) and winter of 2017 (F). In these two cases, the emissions in Beijing were set to zero, while the regional emissions
146 remained at the actual level. The balances between A and E or between B and F represent the contributions of regional transport to
147 the PM_{2.5} concentration in Beijing during the corresponding periods.

148 2.4 Clustering analysis of back trajectories

149 The Hybrid Single Particle Lagrangian Integrated Trajectory (HYSPLIT) model was conducted to calculate the back trajectories
150 of air masses arriving in Beijing during the observation periods in 2014 and 2017. The meteorological input was downloaded from
151 the National Oceanographic and Atmospheric Administration (NOAA) Air Resource Laboratory Archived Global Data
152 Assimilation System (GDAS) (<ftp://arlftp.arlhq.noaa.gov/pub/archives/>). Each trajectory was run for three days, with a time
153 resolution of 1 hour, and the initialized height was 100 m above ground level. In total, 2108 and 1292 trajectories were obtained
154 for the winters of 2014 and 2017, respectively. Based on the built-in clustering calculation, the trajectories were then classified



155 into different groups to represent the main airflows influencing the receptor site. Finally, the optimal 5-cluster and 7-cluster
156 solutions were adopted for the winters of 2014 and 2017, respectively. Details are shown in Fig. S3.

157 2.5 ISORROPIA-II equilibrium calculation

158 The ISORROPIA-II thermodynamic model was used to investigate the effects of particle chemical composition on aerosol
159 properties, i.e., particle pH, AWC, and the partitioning of semivolatile species (Fountoukis and Nenes, 2007). The model computes
160 the equilibrium state of an NH_4^+ - SO_4^{2-} - NO_3^- - Cl^- - Na^+ - Ca^{2+} - K^+ - Mg^{2+} - H_2O inorganic aerosol system with its corresponding gases
161 (Fountoukis and Nenes, 2007). When running the ISORROPIA-II model, it is assumed that the bulk PM_{10} or $\text{PM}_{2.5}$ properties have
162 no compositional dependence on particle size, and aerosols are internally mixed and composed of a single aqueous phase. The
163 validity of these assumptions has been evaluated by a number of studies in various locations (Guo et al., 2015; Weber et al., 2016;
164 M.X. Liu et al., 2017; Li et al., 2018).

165 The model was run in the forward mode by assuming that aerosol solutions were metastable. Particle water associated with OA
166 was not considered in this study given its minor effects. M. X. Liu et al. (2017) showed that organic matter (OM)-induced particle
167 water accounted for only 5% of the total AWC in Beijing. In this study, the transition in aerosol composition was mainly reflected
168 in the variations in nitrate and sulfate concentrations. For the analysis of the sensitivity of aerosol properties to particle composition,
169 a selected sulfate concentration combined with the average temperature, RH, and total ammonia concentration ($\text{NH}_3 + \text{NH}_4^+$)
170 during the winters of 2014 and 2017 was input into the ISORROPIA-II model, where the total nitrate concentration ($\text{HNO}_3 + \text{NO}_3^-$)
171 was left as the free variable.

172 3 Results and discussions

173 3.1 Overall variations in aerosol characteristics from 2014 to 2017

174 Figures S4 and S5 display the temporal variations in meteorological parameters, trace gases, and aerosol species during the two
175 winter campaigns, with the average values shown in Table 1. Compared to the frequently occurring haze episodes in the winter of
176 2014, more clean days with lower PM_{10} concentrations were observed in the winter of 2017. On average, the PM_{10} concentrations
177 were $66.2 \mu\text{g m}^{-3}$ and $33.4 \mu\text{g m}^{-3}$ during the winters of 2014 and 2017, respectively. The large reduction in PM_{10} concentration
178 reflects the effectiveness of pollution abatement strategies. Satellite-derived estimates also showed an evident decrease in $\text{PM}_{2.5}$
179 concentration in North China in recent years (Gui et al., 2019).

180 3.1.1 Changes in SIA characteristics

181 Sulfate, nitrate, and ammonium are the dominant components in SIAs and are generally recognized as ammonium sulfate and
182 ammonium nitrate in $\text{PM}_{2.5}$. With the implementation of clean air actions, sulfate underwent the largest decline in the mass
183 concentration among all SIA species (from $7.7 \mu\text{g m}^{-3}$ to $2.8 \mu\text{g m}^{-3}$ during 2014-2017). The contributions of nitrate and ammonium
184 to PM_{10} mass reduction were $1.3 \mu\text{g m}^{-3}$ and $1.5 \mu\text{g m}^{-3}$, respectively. Different changes in the mass concentration of SIA species
185 led to variations in the PM_{10} chemical composition. As illustrated in Fig. 1, nitrate exhibited an increasing mass fraction in PM_{10}
186 from 18% to 30%, whereas the mass contribution of sulfate decreased from 12% to 8%. Correspondingly, the mass ratio of
187 nitrate/sulfate increased from 1.4 in 2014 to 3.5 in 2017. Based on the measurements in Beijing from November to December, Xu
188 et al. (2018) also observed a higher nitrate/sulfate ratio in 2016 (1.36) than in 2014 (0.72). Similar annual variations in aerosol
189 chemical composition were found in North America over 2000-2016, with an increased proportion of nitrate and a decreased
190 contribution of sulfate (van Donkelaar et al., 2019). The diurnal cycles of SIAs are displayed in Fig. 2. All SIA species showed



191 similar diel trends in the two winters, with increasing concentrations after noon due to enhanced photochemical processes and peak
192 concentrations at night caused by a lower boundary layer height. However, the absolute variations in the SIA mass concentration
193 differed greatly between 2014 and 2017. While the mass concentration of sulfate decreased by a factor of 2-3 in 2017, nitrate and
194 ammonium showed much smaller reductions of 15-40% in their mass concentrations throughout the day.

195 Previous studies have concluded that the dramatically enhanced contribution of sulfate was a main driving factor of winter haze
196 pollution in China (Wang et al., 2014; Wang et al., 2016; H. Y. Li et al., 2017). However, with the emission mitigation efforts, the
197 role of SIA species in aerosol pollution changed significantly. Aerosol pollution was classified into three categories in this study:
198 clean ($PM_{10} \leq 35 \mu\text{g m}^{-3}$), slightly polluted ($35 < PM_{10} \leq 115 \mu\text{g m}^{-3}$), and polluted ($PM_{10} > 115 \mu\text{g m}^{-3}$). The contributions of different
199 pollution levels and the PM_{10} chemical compositions at each pollution level are shown in Fig. 3 for the winters of 2014 and 2017.
200 While the polluted level accounted for 38% of the observation period in the winter of 2014, only 14% of the observation period
201 was recognized as being polluted in the winter of 2017. In 2014, the mass fraction of sulfate in PM_{10} was 16.1% during clean
202 periods. With the increase in pollution level, the contribution of sulfate increased from 10.6% in slightly polluted periods to 13.6%
203 in polluted periods, while the mass fraction of nitrate decreased. In contrast, sulfate comprised a minor fraction of haze development
204 in 2017. It was nitrate that exhibited a substantially increased mass fraction at higher PM_{10} loadings. From clean to polluted periods,
205 the nitrate contribution to PM_{10} increased from 22.6% to 34.9%. These results demonstrated that aerosol pollution in Beijing has
206 gradually changed from sulfate-driven to nitrate-driven in recent years.

207 3.1.2 Changes in OA characteristics

208 In response to the strict emission controls, the mass concentration of organics declined by $\sim 18.5 \mu\text{g m}^{-3}$ from 2014 to 2017, which
209 was mainly caused by OOA ($\sim 6.8 \mu\text{g m}^{-3}$) and CCOA ($\sim 6.0 \mu\text{g m}^{-3}$). The contribution from HOA was $2.6 \mu\text{g m}^{-3}$, which was
210 associated with the strengthened controls on vehicle emissions. BBOA decreased by $3.2 \mu\text{g m}^{-3}$ because the use of traditional
211 biofuels, such as wood and crop residuals, was forbidden in Beijing by the end of 2016. Generally, the concentrations of all OA
212 factors declined substantially throughout the day in 2017. For primary factors, the reductions in their mass concentrations were
213 much higher at night than during the day (Fig. 2). Compared to 2014, CCOA decreased by a factor of 4-5 at night in 2017 and a
214 factor of 1.5 during the day.

215 Overall, the mass fraction of organics in PM_{10} declined from 49% to 36% over the period (Fig. 1). The source apportionment results
216 demonstrated that coal combustion was largely accountable for the reduced contribution of organics. During 2014-2017, the mass
217 fraction of CCOA in the total OA decreased from 27% to 18%. Reports from the Beijing Municipal Environmental Protection
218 Bureau (MEPB) also revealed that the contribution of coal combustion to aerosol pollution showed a large decrease during 2013-
219 2017. The decline in CCOA was largely driven by the reduced emissions of organics from coal combustion with the implementation
220 of clean air actions. In contrast, the mass contribution of OOA in the total OA increased from 41% to 49% during 2014-2017.
221 OOA is formed in the atmosphere through various oxidation reactions of volatile organic compounds (VOCs). From 2013 to 2017,
222 VOCs emissions decreased by approximately half in Beijing but remained constant in the surrounding regions. Large amounts of
223 OOA brought to Beijing via regional transport weakened the efforts of local emission cuts. Therefore, stronger emission controls
224 of VOCs need to be placed in both local Beijing and adjacent areas in the future.

225 3.2 Factors affecting aerosol characteristics from 2014 to 2017

226 3.2.1 Meteorological conditions

227 To evaluate the influence of weather conditions on air quality improvement, we compared the daily changes in meteorological
228 parameters during the winters of 2014 and 2017 (Fig. S6). Compared to 2014, the temperature in 2017 was slightly lower



229 throughout the whole day, which may have facilitated gas-particle conversion for semivolatile species, such as ammonium nitrate.
230 Although the RH was similar between 2014 and 2017 during the daytime, the nighttime RH in 2017 was slightly higher than that
231 in 2014, which was favorable for the heterogeneous reactions of secondary species. On average, the observed RH was 29.6% in
232 the winter of 2014 and 33.9% in the winter of 2017. Diurnal cycles of WS showed that the WS in winter of 2017 was somewhat
233 higher, implying beneficial conditions for the dispersal of air pollutants. To illustrate the variations in WD, the observed data were
234 classified into four groups: from north to east (N-E; $0^\circ \leq \text{WD} < 90^\circ$), east to south (E-S; $90^\circ \leq \text{WD} < 180^\circ$), south to west (S-W;
235 $180^\circ \leq \text{WD} < 270^\circ$), and west to north (W-N; $270^\circ \leq \text{WD} \leq 360^\circ$). As displayed in Fig. S6d, the winters of 2014 and 2017 were
236 both dominated by W-N and N-E, which usually bring clean air masses. After noon, the contribution of winds from S-W started
237 to increase. According to previous studies, southerly winds arriving in Beijing generally carry higher levels of air pollutants from
238 the southern regions (Sun et al., 2006; Zhao et al., 2009).

239 Simulations with the WRF-CMAQ model helped to assess the relative importance of meteorology for changes in aerosol
240 concentration and chemical composition. The effects of meteorology were quantified by comparing cases *A* and *C* or cases *B* and
241 *D*. The differences between *A* and *D* or *B* and *C* reflected the effectiveness of emission control. For the total $\text{PM}_{2.5}$ concentration,
242 the simulation results clearly demonstrated that variations in meteorology from 2014 to 2017 had a much lower influence on the
243 $\text{PM}_{2.5}$ reduction than the changes in air pollutant emissions (Fig. S7). On average, changes in weather conditions resulted in a $\text{PM}_{2.5}$
244 decrease of $9.6 \mu\text{g m}^{-3}$, which explained 24.8% of the total $\text{PM}_{2.5}$ reduction. These results suggest that meteorological variations
245 are far from sufficient to explain $\text{PM}_{2.5}$ abatement during 2014-2017. In terms of aerosol composition, we compared the simulated
246 results of cases *B* and *D* and found that meteorological changes from 2014 to 2017 had a negligible influence on the chemical
247 composition of $\text{PM}_{2.5}$ (Fig. 4). Therefore, we conclude that weather conditions in 2017 marginally favored air quality improvement
248 in Beijing, and emission reductions in air pollutants played a dominant role in the variations in aerosol concentration and
249 composition.

250 3.2.2 Emission changes

251 According to both the observations (Fig. 1) and simulation results (Fig. 5a), sulfate and organics experienced the largest decreases
252 among different components in Beijing from 2014 to 2017, which is consistent with the considerable emission reductions in SO_2
253 and primary OC in local Beijing and its surrounding regions (Fig. 6; i.e., Tianjin, Hebei, Shandong, Henan, Shanxi, and Inner
254 Mongolia). Comparatively, the wintertime nitrate concentration showed the lowest reduction during 2014-2017, which was
255 expected from the smaller emission cut of NO_x in Beijing and its surrounding areas.

256 Based on the bottom-up emission inventories (Zheng et al., 2018; Cheng et al., 2019), SO_2 emissions decreased by 79.9% in Beijing
257 during 2014-2017, mainly due to the effective control of coal combustion sources and the optimization of the energy structure.
258 Until 2017, all coal-fired power units were shut down, and small coal-fired boilers with capacities of <7 MW were eliminated in
259 Beijing, which reduced coal use by more than 17 million tons. In addition, most of the clustered and highly polluted enterprises
260 and factories were phased out during this period. These control measures remarkably reduced SO_2 emissions from power and
261 industry sectors. Enhanced energy restructuring was also implemented in the residential sector. During 2013-2017, more than 2
262 million tons of residential coal was replaced by cleaner natural gas and electricity, involving 900,000 households in Beijing. Apart
263 from coal burning, the use of traditional biomass, such as wood and crops, was thoroughly forbidden in Beijing by the end of 2016.
264 The strict governance of residential fuel also made substantial contributions to the BC and OC emission reductions in Beijing,
265 which decreased by 71.2% and 59.9%, respectively, during 2014-2017. In comparison, NO_x showed a lower emission reduction
266 of 38.1% from 2014 to 2017 in Beijing. The decline in NO_x emissions was mainly caused by the strengthened emission control of
267 on-road and off-road transportation, the shutdown of all coal-fired power plants, and the application of low-nitrogen-burning (LNB)



268 technologies in industrial boilers. However, due to the insufficient end-of-pipe control of widespread gas-fired facilities and the
269 rapid increase in the vehicle population (the number of vehicles in Beijing increased by nearly 10% during 2013-2017), the NO_x
270 emission reduction in Beijing was not as significant as the SO₂ emission reduction.

271 In adjacent regions, SO₂ emissions decreased by 50.6% from 2014 to 2017, while NO_x emissions showed a much smaller reduction
272 of 15.2%. Comparatively, the energy structure adjustments in surrounding areas were less intense than those in Beijing. Emission
273 reductions in SO₂ and NO_x in surrounding regions were mainly attributed to ultralow power plant emissions and the reinforced
274 end-of-pipe control of key industries. Because of the looser emission standards for vehicles and the lack of vehicle management,
275 control measures on transportation in adjacent regions were highly insufficient for NO_x emission reduction compared with those
276 in Beijing. Overall, the observed transition in PM₁ chemical composition with increasing nitrate contribution and decreasing sulfate
277 fraction was in agreement with the emission changes in their precursors.

278 3.2.3 Regional transport

279 Variations in regional weather patterns and emission changes in air pollutants in surrounding regions influenced the effect of
280 regional transport on aerosol characteristics in Beijing. Statistical analysis of air mass trajectories was performed using the
281 HYSPLIT model. Based on the clustering technique, back trajectories were classified into groups of similar length and curvature
282 to identify the main airflows affecting the site. The five-cluster solution and seven-cluster solution were adopted for the winters of
283 2014 and 2017, respectively. The PM₁ mass concentration and mass composition for each cluster are shown in Fig. S8. For a better
284 comparison between 2014 and 2017, clusters were further grouped into two categories according to PM₁ loadings. Clusters arriving
285 in Beijing when the local PM₁ concentration was less than 35 µg m⁻³ were recognized as clean clusters, while clusters with PM₁
286 concentrations greater than 35 µg m⁻³ were defined as polluted clusters. As displayed in Fig. 7, the average PM₁ concentration in
287 local Beijing was 114 µg m⁻³ in 2014 when the polluted clusters arrived, which was much higher than that in 2017 (74 µg m⁻³).
288 While the contribution of polluted clusters in 2014 was 47%, polluted air masses transported from surrounding regions influenced
289 Beijing approximately 20% of the time in 2017. The results here indicate that compared to 2014, Beijing was less influenced by
290 polluted air masses transported from surrounding areas in 2017 during the wintertime, which benefited air quality improvement.
291 In addition, air masses in 2017 brought more nitrate and less sulfate to Beijing than those in 2014.

292 The WRF-CMAQ model simulations showed that the contributions of regional transport to the PM_{2.5} concentration in Beijing were
293 31.4 µg m⁻³ and 19.0 µg m⁻³ in the winters of 2014 and 2017, respectively (Fig. 5b). Although the proportion of regional transport
294 (relative to the total PM_{2.5} concentration in Beijing) remained at approximately 35% in the two winters (34.4% in the winter of
295 2014 and 36.4% in the winter of 2017), the absolute amount decreased by 39.6%. This result further supported that less PM_{2.5}
296 transported from surrounding regions indeed helped with PM_{2.5} abatement in Beijing. Compared with 2014, the variations in PM_{2.5}
297 components due to regional transport (Fig. 5b) in 2017 were basically consistent with the total aerosol composition changes that
298 were observed (Fig. 1) and simulated (Fig. 5a) in Beijing. Sulfate had the most notable decrease, with a decreasing rate of 57.9%,
299 and the regional transport of OM and BC decreased by over 38%. The significant reduction in sulfate was mainly attributed to the
300 effective SO₂ emission controls in the surrounding regions, such as the special emission limits for power plants and the innovation
301 of industrial boilers. The decreasing rate of regional transport OM was obviously lower than the total change, suggesting that the
302 local emission controls of VOCs and primary OM in Beijing had a dominant contribution to the decrease in OM. The reduction in
303 nitrate from regional transport was much smaller than that in other components. This was not only due to the insufficient NO_x
304 emission controls in the surrounding areas but also the relatively rich ammonium environment in North China, which might have
305 weakened the effects of NO_x reductions. Therefore, the collaborative reductions in NO_x and NH₃ are important for future air
306 pollution control strategies (Liu et al., 2019).



307 3.2.4 Formation mechanisms

308 From a traditional viewpoint, sulfate formation mainly includes SO₂ oxidation by OH in the gas phase and SO₂ oxidation in cloud
309 droplets by H₂O₂ and O₃ in the aqueous phase (Seinfeld and Pandis, 2012). This is actually the case for global sulfate production
310 (Roelofs et al., 1998). The formation rate of sulfate through aqueous reactions is typically much faster than that through gas-phase
311 oxidations. Recently, studies have found that the heterogeneous oxidation of SO₂ in aerosol water, which is usually ignored in
312 current model simulations, plays an important role in the persistent formation of sulfate during haze events in China (B. Zheng et
313 al., 2015; Cheng et al., 2016; Wang et al., 2016). However, with the substantial decrease in SO₂ emissions currently, the importance
314 of heterogeneous chemistry in sulfate formation is highly uncertain.

315 To shed light on this query, the formation of sulfate and nitrate with increasing RH was compared between 2014 and 2017. As
316 displayed in Fig. 8, the SO₄/BC ratio was much lower in 2017 than in 2014, especially at a higher RH, indicating greatly weakened
317 sulfate formation in 2017 compared to primary BC emissions. NO₃/BC showed little difference between 2014 and 2017. The
318 oxidation ratios of sulfur and nitrogen were further estimated as SOR (the molar ratio of sulfate to the sum of sulfate and SO₂) and
319 NOR (the molar ratio of nitrate to the sum of nitrate and NO_x), respectively. Median values were used for comparison between
320 2014 and 2017 to avoid bias caused by outliers. When the RH>50%, SOR started to increase significantly with the enhancement
321 in RH in 2014, which was consistent with previous observations in Beijing in 2013 (G. J. Zheng et al., 2015). A year-long study
322 in Beijing from 2012 to 2013 also revealed that a rapid increase in SOR was found at a RH threshold of ~45% (Fang et al., 2019).
323 However, the starting point of SOR growth was clearly delayed in 2017, with a higher RH of 70%. Considering the decrease in
324 the SO₂ mixing ratio from 15.5 ppb in the winter of 2014 to 2.8 ppb in the winter of 2017 (Table 1), the results here imply that
325 with the large reduction in gaseous precursors, the rapid formation of sulfate through heterogeneous reaction is more difficult to
326 occur. In addition to emission reduction, reduced regional transport from southern polluted regions in 2017 helped to lower SO₂
327 concentrations in Beijing. Previous studies have revealed the positive feedback between aerosols and boundary layers, as high
328 aerosol loadings could decrease the boundary layer height and further increase aerosol concentrations (Petäjä et al., 2016; Z. Li et
329 al., 2017). With a lower PM_{2.5} concentration in 2017, the interactions between aerosols and the boundary layer were weakened,
330 which in turn also favored a decrease in the SO₂ concentration. At a lower RH, the SOR in 2017 (~0.14) was unexpectedly higher
331 than that in 2014 (~0.06), demonstrating a higher sulfate production rate in 2017. Similar results have been observed over the
332 eastern United States, where a considerable decrease in SO₂ resulted in the more efficient formation of particulate sulfate during
333 wintertime (Shah et al., 2018). Combining airborne measurements, ground-based observations, and GEOS-Chem simulations, Shah
334 et al. (2018) explained that sulfate production in winter is limited by the availability of oxidants and particle acidity. At lower
335 concentrations of precursor gases, the oxidant limitation on SO₂ oxidation weakened, leading to a higher formation rate of sulfate.
336 Particulate nitrate in PM_{2.5} is mainly formed through the neutralization of HNO₃ with NH₃. HNO₃ is produced by NO₂ oxidation
337 via OH during the day and the hydrolysis reaction of dinitrogen pentoxide (N₂O₅) at night, with the former being the dominant
338 pathway (Alexander et al., 2009). At a lower RH, NOR was slightly higher in 2017 than in 2014 (Fig. 8), which may have been
339 caused by the reduced limitation of oxidants with lower NO_x emissions in 2017. Nitrate formation was also affected by the
340 competition for available NH₃ between sulfate and nitrate. In the atmosphere, NH₃ prefers to react first with H₂SO₄ to form
341 ammonium sulfate due to its stability. When excess NH₃ is available, ammonium nitrate is formed (Seinfeld and Pandis, 2012).
342 With the decrease in sulfate concentration in 2017, some NH₃ was freed up to react with HNO₃. This may have also facilitated the
343 formation rate of nitrate. When RH>60%, NOR increased substantially in 2014 and 2017, indicating the importance of
344 heterogeneous reactions in nitrate production.



3.3 Influence of the transition in aerosol characteristics on particle properties

According to thermodynamic calculations, various aerosol properties were affected by changes in aerosol characteristics associated with clean air actions. As shown in Fig. 9a, nitrate and sulfate play key roles in determining the AWC in $PM_{2.5}$. The decreasing mass concentrations of nitrate and sulfate result in a lower AWC. Similar observations have been reported previously across northern China, revealing that nitrate and sulfate are dominant anthropogenic inorganic salts driving AWC (Wu et al., 2018). With the clean air actions enacted, the mass concentrations of nitrate and sulfate decreased during 2013-2017, leading to an average decline in AWC from 4.8 to 2.5 $\mu\text{g m}^{-3}$. Data for the winter of 2013 were acquired from Sun et al. (2016). The reduced AWC further helped air quality improvement by lowering the ambient aerosol mass and enhancing visibility. Because aqueous-phase reactions contribute largely to sulfate formation in winter, the decrease in AWC decelerated the formation of sulfate. In addition, the lower AWC slowed down the uptake coefficient of N_2O_5 for heterogeneous processing, thereby suppressing the formation of particulate nitrate.

Figure 9b displays the effects of nitrate and sulfate concentrations on particle acidity. Particle acidity is largely driven by the mass concentration of sulfate and is less sensitive to the variation in nitrate. Particle pH substantially decreases with increasing sulfate concentration. In contrast, more particulate nitrate leads to a slightly higher pH by increasing the particle liquid water and diluting aqueous H^+ concentrations. Through the comparison of pH predictions among various locations worldwide, Guo et al. (2018) also found that a higher particle pH was generally associated with higher concentrations of nitrate. During 2013-2017, the average particle pH varied from 5.0 to 6.2, with a significant decrease in sulfate concentration, resulting in a more neutral atmospheric environment. When $pH > 5.0$, aqueous-phase productions of sulfate are dominated by SO_2 oxidation with H_2O_2 , O_3 , and NO_2 under haze conditions in Beijing (Cheng et al., 2016). The sulfate oxidation rates by O_3 and NO_2 increase with increasing particle pH. Therefore, a more neutral atmosphere would favor aqueous-phase sulfate formation in Beijing. Particle acidity also influences the gas-particle partitioning of nitrate. The rising particle pH would result in a higher fraction of particulate nitrate ($\epsilon(NO_3^-) = \frac{[NO_3^-]}{[HNO_3] + [NO_3^-]}$). Figure S9a displays the variation in $\epsilon(NO_3^-)$ as a function of particle pH under typical Beijing winter conditions (temperature of approximately 0°C). With a particle pH below 3, $\epsilon(NO_3^-)$ increases sufficiently with the enhancement in particle pH. However, when the particle pH is larger than 3, $\epsilon(NO_3^-)$ remains relatively stable (approaching 1). From 2013 to 2017, with the particle pH remaining above 3 in Beijing, no clear change in $\epsilon(NO_3^-)$ was observed (Fig. S9b).

The variations in nitrate and sulfate concentrations also affected the gas-particle partitioning of total ammonium ($NH_x = NH_3 + NH_4^+$). As expected, the decreased concentrations of nitrate and sulfate led to a reduction in the ammonium particle fraction ($\epsilon(NH_4^+) = NH_4^+ / NH_x$; Fig. 10). From 2013 to 2017, $\epsilon(NH_4^+)$ in Beijing always stayed below 0.3, indicating that most ammonium existed in the gas phase. Therefore, a minor reduction in NH_x would not be sufficient for air quality improvement. Guo et al. (2018) revealed that for winter haze conditions in Beijing, an approximate 60% decrease in NH_x was required to achieve an effective reduction in $PM_{2.5}$. Due to the close linkage between ammonia emissions and agricultural activities, it may be difficult to attain substantial ammonia reduction in China.

4 Conclusions

This study investigated the variations in aerosol characteristics in Beijing during the winters of 2014 and 2017 by combining the online measurements of aerosol chemical composition with a comprehensive model analysis of meteorological conditions, anthropogenic emissions, and regional transport. The average PM_1 concentration decreased from 66.2 $\mu\text{g m}^{-3}$ in the winter of 2014 to 33.4 $\mu\text{g m}^{-3}$ in the winter of 2017, with decreasing concentrations of organics, sulfate, nitrate, and ammonium by 18.5 $\mu\text{g m}^{-3}$, 4.9 $\mu\text{g m}^{-3}$, 1.3 $\mu\text{g m}^{-3}$, and 1.5 $\mu\text{g m}^{-3}$, respectively. These changes reduced the mass fractions of organics and sulfate from 59%



383 to 36% and from 13% to 9%, respectively, whereas increased the nitrate contribution from 19% to 32%. Consequently, the winter
384 haze pollution changed from sulfate-driven to nitrate-driven in Beijing from 2014 to 2017, implicating the increasing role of nitrate
385 in aerosol pollution.

386 The chemical transport model simulations suggest that the rapidly declining emissions in Beijing and its adjacent regions account
387 for ~75% of PM_{2.5} abatement in Beijing, and the remaining portion can be explained by the favorable weather conditions in 2017.
388 The faster reductions in SO₂ emissions compared to NO_x emissions are in line with the decreased sulfate contribution and increased
389 nitrate fraction in observed aerosols, and the model simulations with these emission estimates can reproduce the relative changes
390 in aerosol composition. Regional transport contributed moderately to the variations in aerosol concentration and its chemical
391 composition, with less polluted air masses transported from surrounding regions to Beijing in the winter of 2017. The air masses
392 were observed to have brought more nitrate and less sulfate to Beijing. Furthermore, the considerable decrease in SO₂ emissions
393 suppressed the rapid formation of sulfate during wintertime. The fast SO₂-to-sulfate conversion through heterogeneous reactions
394 was observed to increase promptly at a RH threshold of ~50% in 2014, while a higher RH of 70% was observed in 2017.

395 Thermodynamic calculations showed that the decreased sulfate and nitrate concentrations in 2017 caused a lower AWC in PM_{2.5},
396 which further decreased the ambient aerosol mass and weakened the formation rates of sulfate and nitrate through aqueous-phase
397 reactions. Particle acidity displayed a decline during 2014–2017, mostly driven by the declining sulfate concentration. In turn, the
398 more neutral ambient environment would favor the aqueous oxidation of sulfate in Beijing. Analysis of the ammonium particle
399 fraction indicated that most ammonium in Beijing existed in the gas phase. Therefore, increased efforts are needed to achieve an
400 effective reduction in particle ammonium in the future.

401 **Author contributions**

402 QZ and KH conceived the study. HL conducted the field measurements and carried out the data analysis. JC provided the emission
403 data and performed the model simulations. BZ participated the data analysis. HL, JC and QZ wrote the paper with inputs from all
404 coauthors.

405 **Acknowledgements**

406 This work was funded by the National Natural Science Foundation of China (41571130035, 41571130032 and 41625020).

407 **References**

- 408 Bey, I., Jacob, D. J., Yantosca, R. M., Logan, J. A., Field, B. D., Fiore, A. M., Li, Q., Liu, H., Mickley, L. J., and Schultz, M. G.:
409 Global modeling of tropospheric chemistry with assimilated meteorology: Model description and evaluation, *J. Geophys. Res.*,
410 106, D19, 23073–23095, <https://doi.org/10.1029/2001JD000807>, 2001.
- 411 Canonaco, F., Crippa, M., Slowik, J. G., Baltensperger, U., and Prevot, A. S. H.: SoFi, an IGOR-based interface for the efficient
412 use of the generalized multilinear engine (ME-2) for the source apportionment: ME-2 application to aerosol mass spectrometer
413 data, *Atmos Meas Tech*, 6, 3649–3661, 2013.
- 414 Cheng, J., Su, J., Cui, T., Li, X., Dong, X., Sun, F., Yang, Y., Tong, D., Zheng, Y., Li, Y., Li, J., Zhang, Q., and He, K.: Dominant
415 role of emission reduction in PM_{2.5} air quality improvement in Beijing during 2013–2017: a model-based decomposition
416 analysis, *Atmos. Chem. Phys.*, 19, 6125–6146, <https://doi.org/10.5194/acp-19-6125-2019>, 2019.
- 417 Cheng, Y. F., Zheng, G. J., Wei, C., Mu, Q., Zheng, B., Wang, Z. B., Gao, M., Zhang, Q., He, K. B., Carmichael, G., Poschl, U.,
418 and Su, H.: Reactive nitrogen chemistry in aerosol water as a source of sulfate during haze events in China, *Sci Adv*, 2, 2016.



- 419 Cohen, A. J., Brauer, M., Burnett, R., Anderson, H. R., Frostad, J., Estep, K., Balakrishnan, K., Brunekreef, B., Dandona, L.,
420 Dandona, R., Feigin, V., Freedman, G., Hubbell, B., Jobling, A., Kan, H., Knibbs, L., Liu, Y., Martin, R., Morawska, L., Pope,
421 C. A., Shin, H., Straif, K., Shaddick, G., Thomas, M., van Dingenen, R., van Donkelaar, A., Vos, T., Murray, C. J. L., and
422 Forouzanfar, M. H.: Estimates and 25-year trends of the global burden of disease attributable to ambient air pollution: an
423 analysis of data from the Global Burden of Diseases Study 2015, *Lancet*, 389, 1907-1918, 2017.
- 424 Fang, Y., Ye, C., Wang, J., Wu, Y., Hu, M., Lin, W., Xu, F., and Zhu, T.: RH and O₃ concentration as two prerequisites for sulfate
425 formation, *Atmos. Chem. Phys. Discuss.*, 2019, 1-25, 10.5194/acp-2019-284, 2019.
- 426 Fountoukis, C., and Nenes, A.: ISORROPIA II: a computationally efficient thermodynamic equilibrium model for K⁺-Ca²⁺-Mg²⁺-
427 NH₄⁺-Na⁺-SO₄²⁻-NO₃⁻-Cl-H₂O aerosols, *Atmos Chem Phys*, 7, 4639-4659, 2007.
- 428 Gao, M., Carmichael, G. R., Saide, P. E., Lu, Z., Yu, M., Streets, D. G., and Wang, Z.: Response of winter fine particulate matter
429 concentrations to emission and meteorology changes in North China, *Atmos. Chem. Phys.*, 16, 11837-11851, 10.5194/acp-
430 16-11837-2016, 2016.
- 431 Geng, G., Zhang, Q., Tong, D., Li, M., Zheng, Y., Wang, S., and He, K.: Chemical composition of ambient PM_{2.5} over China
432 and relationship to precursor emissions during 2005–2012, *Atmos. Chem. Phys.*, 17, 9187-9203, 10.5194/acp-17-9187-2017,
433 2017.
- 434 Gui, K., Che, H., Wang, Y., Wang, H., Zhang, L., Zhao, H., Zheng, Y., Sun, T., and Zhang, X.: Satellite-derived PM_{2.5}
435 concentration trends over Eastern China from 1998 to 2016: Relationships to emissions and meteorological parameters,
436 *Environ Pollut*, 247, 1125-1133, <https://doi.org/10.1016/j.envpol.2019.01.056>, 2019.
- 437 Guo, H., Xu, L., Bougiatioti, A., Cerully, K. M., Capps, S. L., Hite, J. R., Carlton, A. G., Lee, S. H., Bergin, M. H., Ng, N. L.,
438 Nenes, A., and Weber, R. J.: Fine-particle water and pH in the southeastern United States, *Atmos Chem Phys*, 15, 5211-5228,
439 2015.
- 440 Guo, H. Y., Otjes, R., Schlag, P., Kiendler-Scharr, A., Nenes, A., and Weber, R. J.: Effectiveness of ammonia reduction on control
441 of fine particle nitrate, *Atmos Chem Phys*, 18, 12241-12256, 2018.
- 442 Huang, X. F., He, L. Y., Hu, M., Canagaratna, M. R., Sun, Y., Zhang, Q., Zhu, T., Xue, L., Zeng, L. W., Liu, X. G., Zhang, Y. H.,
443 Jayne, J. T., Ng, N. L., and Worsnop, D. R.: Highly time-resolved chemical characterization of atmospheric submicron
444 particles during 2008 Beijing Olympic Games using an Aerodyne High-Resolution Aerosol Mass Spectrometer, *Atmos Chem*
445 *Phys*, 10, 8933-8945, 2010.
- 446 Intergovernmental Panel on Climate Change (IPCC) (2013), *Climate Change 2013: The Physical Science Basis. Contribution of*
447 *Working Group I to the Fifth Assessment Report of the Intergovernmental Panel on Climate Change*, 1535 pp., Cambridge
448 Univ. Press, Cambridge, U. K., and New York.
- 449 Li, H. Y., Zhang, Q., Zhang, Q., Chen, C. R., Wang, L. T., Wei, Z., Zhou, S., Parworth, C., Zheng, B., Canonaco, F., Prevot, A. S.
450 H., Chen, P., Zhang, H. L., Wallington, T. J., and He, K. B.: Wintertime aerosol chemistry and haze evolution in an extremely
451 polluted city of the North China Plain: significant contribution from coal and biomass combustion, *Atmos Chem Phys*, 17,
452 4751-4768, 2017.
- 453 Li, H. Y., Zhang, Q., Zheng, B., Chen, C. R., Wu, N. N., Guo, H. Y., Zhang, Y. X., Zheng, Y. X., Li, X., and He, K. B.: Nitrate-
454 driven urban haze pollution during summertime over the North China Plain, *Atmos Chem Phys*, 18, 5293-5306, 2018.
- 455 Li, M., Zhang, Q., Kurokawa, J. I., Woo, J. H., He, K., Lu, Z., Ohara, T., Song, Y., Streets, D. G., Carmichael, G. R., Cheng, Y.,
456 Hong, C., Huo, H., Jiang, X., Kang, S., Liu, F., Su, H., and Zheng, B.: MIX: a mosaic Asian anthropogenic emission inventory
457 under the international collaboration framework of the MICS-Asia and HTAP, *Atmos. Chem. Phys.*, 17, 935-963,
458 <https://doi.org/10.5194/acp-17-935-2017>, 2017.
- 459 Li, Z., Guo, J., Ding, A., Liao, H., Liu, J., Sun, Y., Wang, T., Xue, H., Zhang, H., and Zhu, B.: Aerosol and boundary-layer
460 interactions and impact on air quality, *National Science Review*, 4, 810-833, 10.1093/nsr/nwx117 %J National Science
461 Review, 2017.
- 462 Liang, P. F., Zhu, T., Fang, Y. H., Li, Y. R., Han, Y. Q., Wu, Y. S., Hu, M., and Wang, J. X.: The role of meteorological conditions
463 and pollution control strategies in reducing air pollution in Beijing during APEC 2014 and Victory Parade 2015, *Atmos Chem*
464 *Phys*, 17, 2017.
- 465 Liu, M. M., Bi, J., and Ma, Z. W.: Visibility-Based PM_{2.5} Concentrations in China: 1957-1964 and 1973-2014, *Environmental*
466 *Science & Technology*, 51, 13161-13169, 2017.



- 467 Liu, M. X., Song, Y., Zhou, T., Xu, Z. Y., Yan, C. Q., Zheng, M., Wu, Z. J., Hu, M., Wu, Y. S., and Zhu, T.: Fine particle pH
468 during severe haze episodes in northern China, *Geophys Res Lett*, 44, 5213-5221, 2017.
- 469 Liu, M. X., Huang, X., Song, Y., Tang, J., Cao, J., Zhang, X., Zhang, Q., Wang, S., Xu, T., Kang, L., Cai, X., Zhang, H., Yang, F.,
470 Wang, H., Yu, J., Lau, Alexis K. H., He, L., Huang, X., Duan, L., Ding A., Xue, L., Gao, J., Liu, B., and Zhu, T.: Ammonia
471 emission control in China would mitigate haze pollution and nitrogen deposition, but worsen acid rain, *PANS*, 116 (16) 7760-
472 7765, <https://doi.org/10.1073/pnas.1814880116>, 2019.
- 473 Middlebrook, A. M., Bahreini, R., Jimenez, J. L., and Canagaratna, M. R.: Evaluation of Composition-Dependent Collection
474 Efficiencies for the Aerodyne Aerosol Mass Spectrometer using Field Data, *Aerosol Sci Tech*, 46, 258-271, 2012. Ng, N. L.,
475 Herndon, S. C., Trimborn, A., Canagaratna, M. R., Croteau, P. L., Onasch, T. B., Sueper, D., Worsnop, D. R., Zhang, Q., Sun,
476 Y. L., and Jayne, J. T.: An Aerosol Chemical Speciation Monitor (ACSM) for Routine Monitoring of the Composition and
477 Mass Concentrations of Ambient Aerosol, *Aerosol Sci Tech*, 45, 780-794, 2011a.
- 478 Ng, N. L., Canagaratna, M. R., Jimenez, J. L., Zhang, Q., Ulbrich, I. M., and Worsnop, D. R.: Real-Time Methods for Estimating
479 Organic Component Mass Concentrations from Aerosol Mass Spectrometer Data, *Environmental Science & Technology*, 45,
480 910-916, 2011b.
- 481 Paatero, P.: The multilinear engine - A table-driven, least squares program for solving multilinear problems, including the n-way
482 parallel factor analysis model, *J Comput Graph Stat*, 8, 854-888, 1999.
- 483 Petäjä, T., Järvi, L., Kerminen, V. M., Ding, A. J., Sun, J. N., Nie, W., Kujansuu, J., Virkkula, A., Yang, X., Fu, C. B., Zilitinkevich,
484 S., and Kulmala, M.: Enhanced air pollution via aerosol-boundary layer feedback in China, *Scientific Reports*, 6, 18998,
485 10.1038/srep18998 <https://www.nature.com/articles/srep18998#supplementary-information>, 2016.
- 486 Petzold, A., and Schonlinner, M.: Multi-angle absorption photometry - a new method for the measurement of aerosol light
487 absorption and atmospheric black carbon, *J Aerosol Sci*, 35, 421-441, 2004.
- 488 Pope, C. A., Ezzati, M., and Dockery, D. W.: Fine-Particulate Air Pollution and Life Expectancy in the United States., *New Engl*
489 *J Med*, 360, 376-386, 2009.
- 490 Pui, D. Y. H., Chen, S. C., and Zuo, Z. L.: PM_{2.5} in China: Measurements, sources, visibility and health effects, and mitigation,
491 *Particuology*, 13, 1-26, 2014.
- 492 Roelofs, G.-J. A. N., Lelieveld, J. O. S., and Ganzeveld, L.: Simulation of global sulfate distribution and the influence on effective
493 cloud drop radii with a coupled photochemistry sulfur cycle model, *Tellus B*, 50, 224-242, 10.1034/j.1600-0889.1998.t01-2-
494 00002.x, 1998.
- 495 Seinfeld, J. H. and Pandis, S. N.: Atmospheric chemistry and physics: from air pollution to climate change, 2nd Edition, John
496 Wiley & Sons, New York, USA, 2012.
- 497 Shah, V., Jaegle, L., Thornton, J. A., Lopez-Hilfiker, F. D., Lee, B. H., Schroder, J. C., Campuzano-Jost, P., Jimenez, J. L., Guo,
498 H. Y., Sullivan, A. P., Weber, R. J., Green, J. R., Fiddler, M. N., Bililign, S., Campos, T. L., Stell, M., Weinheimer, A. J.,
499 Montzka, D. D., and Brown, S. S.: Chemical feedbacks weaken the wintertime response of particulate sulfate and nitrate to
500 emissions reductions over the eastern United States, *P Natl Acad Sci USA*, 115, 8110-8115, 2018.
- 501 Squizzato, S., Masiol, M., Brunelli, A., Pistollato, S., Tarabotti, E., Rampazzo, G., and Pavoni, B.: Factors determining the
502 formation of secondary inorganic aerosol: a case study in the Po Valley (Italy), *Atmos Chem Phys*, 13, 1927-1939, 2013.
- 503 Su, X., Tie, X. X., Li, G. H., Cao, J. J., Huang, R. J., Feng, T., Long, X., and Xu, R. G.: Effect of hydrolysis of N₂O₅ on nitrate
504 and ammonium formation in Beijing China: WRF-Chem model simulation, *Sci Total Environ*, 579, 221-229, 2017.
- 505 Sun, J., Liang, M., Shi, Z., Shen, F., Li, J., Huang, L., Ge, X., Chen, Q., Sun, Y., Zhang, Y., Chang, Y., Ji, D., Ying, Q., Zhang,
506 H., Kota, S. H., and Hu, J.: Investigating the PM_{2.5} mass concentration growth processes during 2013–2016 in Beijing and
507 Shanghai, *Chemosphere*, 221, 452-463, <https://doi.org/10.1016/j.chemosphere.2018.12.200>, 2019.
- 508 Sun, Y. L., Zhuang, G. S., Tang, A. H., Wang, Y., and An, Z. S.: Chemical characteristics of PM_{2.5} and PM₁₀ in haze-fog episodes
509 in Beijing, *Environmental Science & Technology*, 40, 3148-3155, 10.1021/es051533g, 2006.
- 510 Sun, Y., Jiang, Q., Wang, Z., Fu, P., Li, J., Yang, T., and Yin, Y.: Investigation of the sources and evolution processes of severe
511 haze pollution in Beijing in January 2013, *Journal of Geophysical Research: Atmospheres*, 119, 4380-4398,
512 10.1002/2014JD021641, 2014.



- 513 Sun, Y. L., Wang, Z. F., Du, W., Zhang, Q., Wang, Q. Q., Fu, P. Q., Pan, X. L., Li, J., Jayne, J., and Worsnop, D. R.: Long-term
514 real-time measurements of aerosol particle composition in Beijing, China: seasonal variations, meteorological effects, and
515 source analysis, *Atmos. Chem. Phys.*, 15, 10149-10165, [10.5194/acp-15-10149-2015](https://doi.org/10.5194/acp-15-10149-2015), 2015.
- 516 Sun, Y. L., Du, W., Fu, P. Q., Wang, Q. Q., Li, J., Ge, X. L., Zhang, Q., Zhu, C. M., Ren, L. J., Xu, W. Q., Zhao, J., Han, T. T.,
517 Worsnop, D. R., and Wang, Z. F.: Primary and secondary aerosols in Beijing in winter: sources, variations and processes,
518 *Atmos Chem Phys*, 16, 8309-8329, 2016.
- 519 Tang, I. N., and Munkelwitz, H. R.: Aerosol Phase-Transformation and Growth in the Atmosphere, *J Appl Meteorol*, 33, 791-796,
520 1994.
- 521 Ulbrich, I. M., Canagaratna, M. R., Zhang, Q., Worsnop, D. R., and Jimenez, J. L.: Interpretation of organic components from
522 Positive Matrix Factorization of aerosol mass spectrometric data, *Atmos Chem Phys*, 9, 2891-2918, 2009.
- 523 van Donkelaar, A., Martin, R. V., Li, C., and Burnett, R. T.: Regional Estimates of Chemical Composition of Fine Particulate
524 Matter Using a Combined Geoscience-Statistical Method with Information from Satellites, Models, and Monitors,
525 *Environmental Science & Technology*, [10.1021/acs.est.8b06392](https://doi.org/10.1021/acs.est.8b06392), 2019. Wang, G. H., Zhang, R. Y., Gomez, M. E., Yang, L.
526 X., Zamora, M. L., Hu, M., Lin, Y., Peng, J. F., Guo, S., Meng, J. J., Li, J. J., Cheng, C. L., Hu, T. F., Ren, Y. Q., Wang, Y.
527 S., Gao, J., Cao, J. J., An, Z. S., Zhou, W. J., Li, G. H., Wang, J. Y., Tian, P. F., Marrero-Ortiz, W., Secrest, J., Du, Z. F.,
528 Zheng, J., Shang, D. J., Zeng, L. M., Shao, M., Wang, W. G., Huang, Y., Wang, Y., Zhu, Y. J., Li, Y. X., Hu, J. X., Pan, B.,
529 Cai, L., Cheng, Y. T., Ji, Y. M., Zhang, F., Rosenfeld, D., Liss, P. S., Duce, R. A., Kolb, C. E., and Molina, M. J.: Persistent
530 sulfate formation from London Fog to Chinese haze, *P Natl Acad Sci USA*, 113, 13630-13635, 2016.
- 531 Wang, X. Y., Wang, K. C., and Su, L. Y.: Contribution of Atmospheric Diffusion Conditions to the Recent Improvement in Air
532 Quality in China, *Scientific Reports*, 6, 2016.
- 533 Wang, Y., Zhang, Q., Jiang, J., Zhou, W., Wang, B., He, K., Duan, F., Zhang, Q., Philip, S., and Xie, Y.: Enhanced sulfate formation
534 during China's severe winter haze episode in January 2013 missing from current models, 119, 10,425-410,440,
535 [doi:10.1002/2013JD021426](https://doi.org/10.1002/2013JD021426), 2014.
- 536 Weber, R. J., Guo, H. Y., Russell, A. G., and Nenes, A.: High aerosol acidity despite declining atmospheric sulfate concentrations
537 over the past 15 years, *Nat Geosci*, 9, 282+, 2016.
- 538 Wu, Z. J., Wang, Y., Tan, T. Y., Zhu, Y. S., Li, M. R., Shang, D. J., Wang, H. C., Lu, K. D., Guo, S., Zeng, L. M., and Zhang, Y.
539 H.: Aerosol Liquid Water Driven by Anthropogenic Inorganic Salts: Implying Its Key Role in Haze Formation over the North
540 China Plain, *Environ Sci Tech Let*, 5, 160-166, 2018.
- 541 Xu, W. Q., Sun, Y. L., Chen, C., Du, W., Han, T. T., Wang, Q. Q., Fu, P. Q., Wang, Z. F., Zhao, X. J., Zhou, L. B., Ji, D. S., Wang,
542 P. C., and Worsnop, D. R.: Aerosol composition, oxidation properties, and sources in Beijing: results from the 2014 Asia-
543 Pacific Economic Cooperation summit study, *Atmos. Chem. Phys.*, 15, 13681-13698, [10.5194/acp-15-13681-2015](https://doi.org/10.5194/acp-15-13681-2015), 2015.
- 544 Xu, W., Sun, Y., Wang, Q., Zhao, J., Wang, J., Ge, X., Xie, C., Zhou, W., Du, W., Li, J., Fu, P., Wang, Z., Worsnop, D. R., and
545 Coe, H.: Changes in Aerosol Chemistry from 2014 to 2016 in Winter in Beijing: Insights from High Resolution Aerosol Mass
546 Spectrometry, 0, [doi:10.1029/2018JD029245](https://doi.org/10.1029/2018JD029245), 2018.
- 547 Yun, H., Wang, W. H., Wang, T., Xia, M., Yu, C., Wang, Z., Poon, S. C. N., Yue, D. L., and Zhou, Y.: Nitrate formation from
548 heterogeneous uptake of dinitrogen pentoxide during a severe winter haze in southern China, *Atmos Chem Phys*, 18, 17515-
549 17527, 2018.
- 550 Zhang, Q., Jimenez, J. L., Canagaratna, M. R., Ulbrich, I. M., Ng, N. L., Worsnop, D. R., and Sun, Y. L.: Understanding
551 atmospheric organic aerosols via factor analysis of aerosol mass spectrometry: a review, *Anal Bioanal Chem*, 401, 3045-3067,
552 2011.
- 553 Zhao, X. J., Zhang, X. L., Xu, X. F., Xu, J., Meng, W., and Pu, W. W.: Seasonal and diurnal variations of ambient PM_{2.5}
554 concentration in urban and rural environments in Beijing, *Atmos Environ*, 43, 2893-2900, [10.1016/j.atmosenv.2009.03.009](https://doi.org/10.1016/j.atmosenv.2009.03.009),
555 2009.
- 556 Zheng, B., Zhang, Q., Zhang, Y., He, K. B., Wang, K., Zheng, G. J., Duan, F. K., Ma, Y. L., and Kimoto, T.: Heterogeneous
557 chemistry: a mechanism missing in current models to explain secondary inorganic aerosol formation during the January 2013
558 haze episode in North China, *Atmos Chem Phys*, 15, 2031-2049, 2015.
- 559 Zheng, B., Tong, D., Li, M., Liu, F., Hong, C., Geng, G., Li, H., Li, X., Peng, L., Qi, J., Yan, L., Zhang, Y., Zhao, H., Zheng, Y.,
560 He, K., and Zhang, Q.: Trends in China's anthropogenic emissions since 2010 as the consequence of clean air actions, *Atmos.*
561 *Chem. Phys.*, 18, 14095-14111, <https://doi.org/10.5194/acp-18-14095-2018>, 2018.



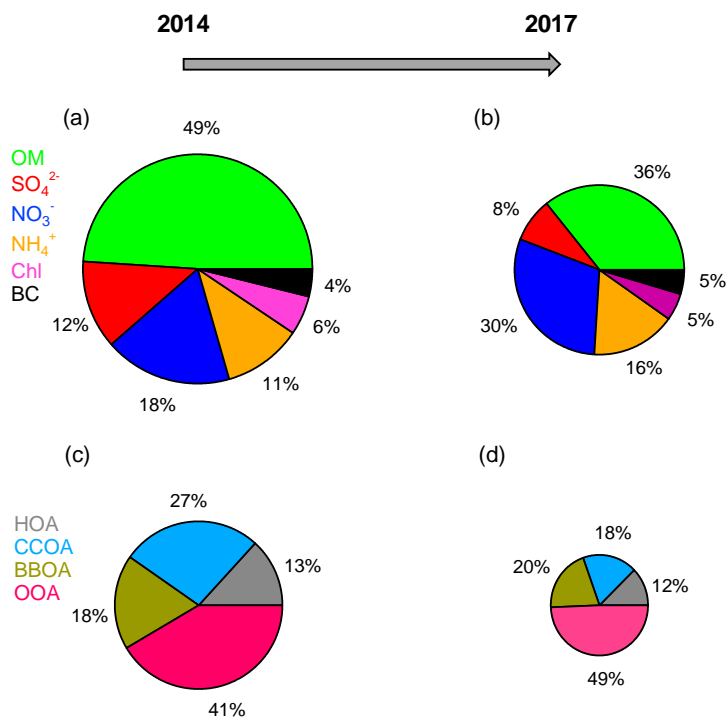
- 562 Zheng, J., Hu, M., Peng, J. F., Wu, Z. J., Kumar, P., Li, M. R., Wang, Y. J., and Guo, S.: Spatial distributions and chemical
563 properties of PM_{2.5} based on 21 field campaigns at 17 sites in China, *Chemosphere*, 159, 480-487, 2016.
- 564 Zheng, G. J., Duan, F. K., Su, H., Ma, Y. L., Cheng, Y., Zheng, B., Zhang, Q., Huang, T., Kimoto, T., Chang, D., Poschl, U.,
565 Cheng, Y. F., and He, K. B.: Exploring the severe winter haze in Beijing: the impact of synoptic weather, regional transport
566 and heterogeneous reactions, *Atmos Chem Phys*, 15, 2969-2983, 2015.



567 **Table 1** Summary of the average meteorological parameters, mixing ratios of gaseous species, and mass concentrations of the PM₁ chemical
 568 components during the winters of 2014 and 2017.

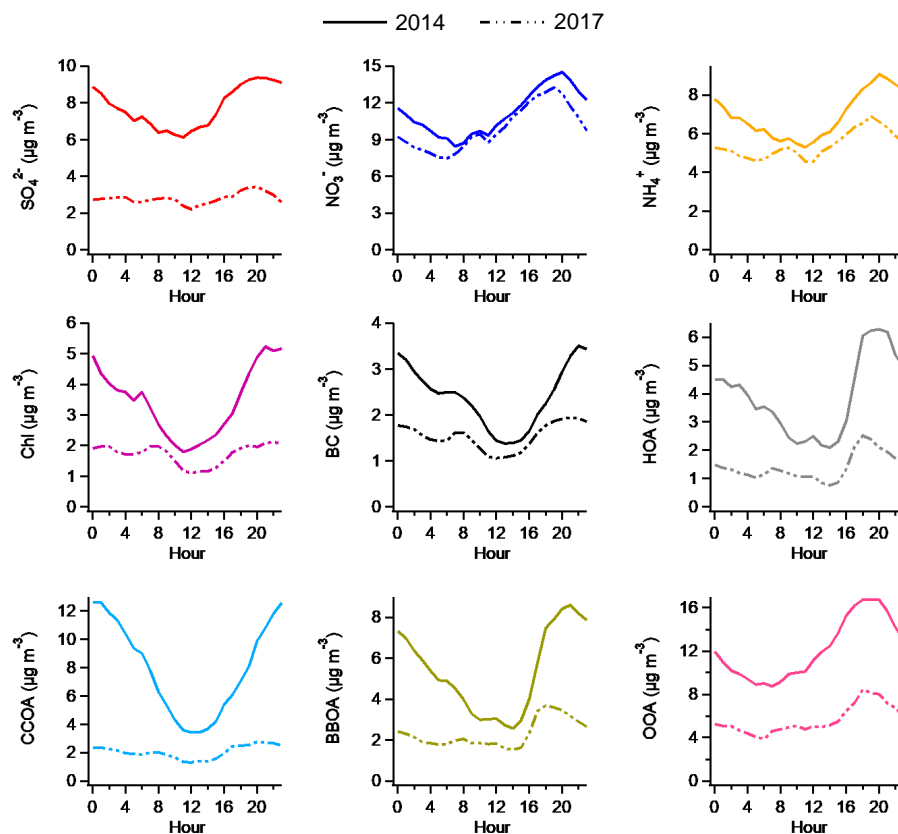
Sampling period		2014 winter	2017 winter
Meteorological parameters	T (°C)	1.70	-2.26
	RH (%)	29.6	33.9
	WS (m s ⁻¹)	1.58	1.73
Gaseous species	SO ₂ (ppb)	15.5	2.8
	NO ₂ (ppb)	26.0	24.9
	CO (ppm)	1.6	0.7
	O ₃ (ppb)	14.4	15.5
Aerosol species (µg m ⁻³)	Org	30.4	11.9
	HOA	4.1	1.5
	BBOA	5.6	2.4
	CCOA	8.2	2.2
	OOA	12.6	5.8
	SO ₄	7.8	2.8
	NO ₃	11.2	9.9
	NH ₄	6.9	5.4
	Chl	3.4	1.7
	BC	2.4	1.5
	PM ₁	66.2	33.4

569



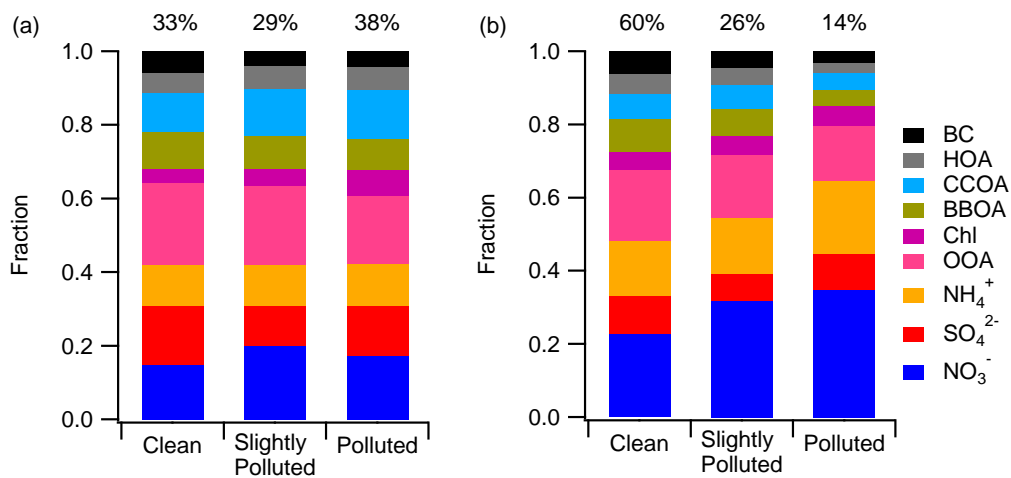
570

571 **Figure 1.** Average chemical compositions of PM₁ and OA in (a, c) winter of 2014 and (b, d) winter of 2017. The decreasing rates of
 572 different components from 2014 to 2017 are as follows: 60.9% for organics, 64.1% for sulfate, 11.6% for nitrate, 21.7% for ammonium,
 573 50.0% for chloride, and 37.5% for BC.



574

575 Figure 2. Average diurnal cycles of different aerosol species in the winter of 2014 (solid line) and winter of 2017 (dashed line).

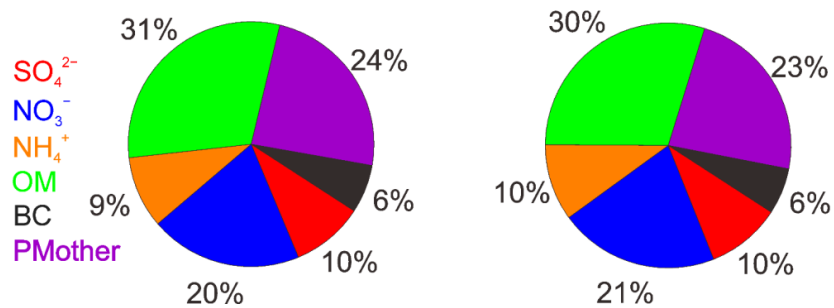


576

577 **Figure 3. Aerosol chemical composition at different pollution levels in the (a) winter of 2014 and (b) winter of 2017. The contributions of**
 578 **each pollution level are shown at the top of each bar.**

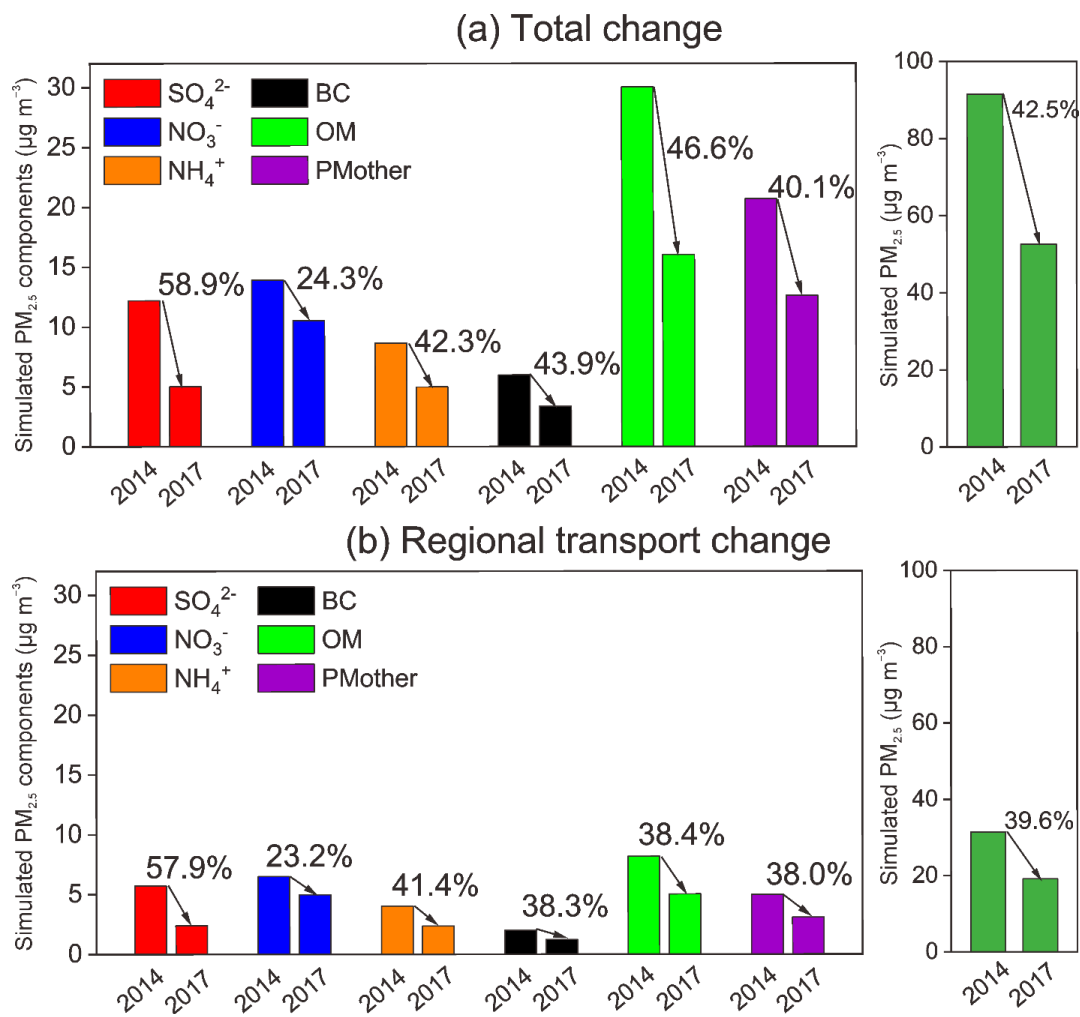


(a) 2017 Emission+2017 Meteorology (b) 2017 Emission+2014 Meteorology



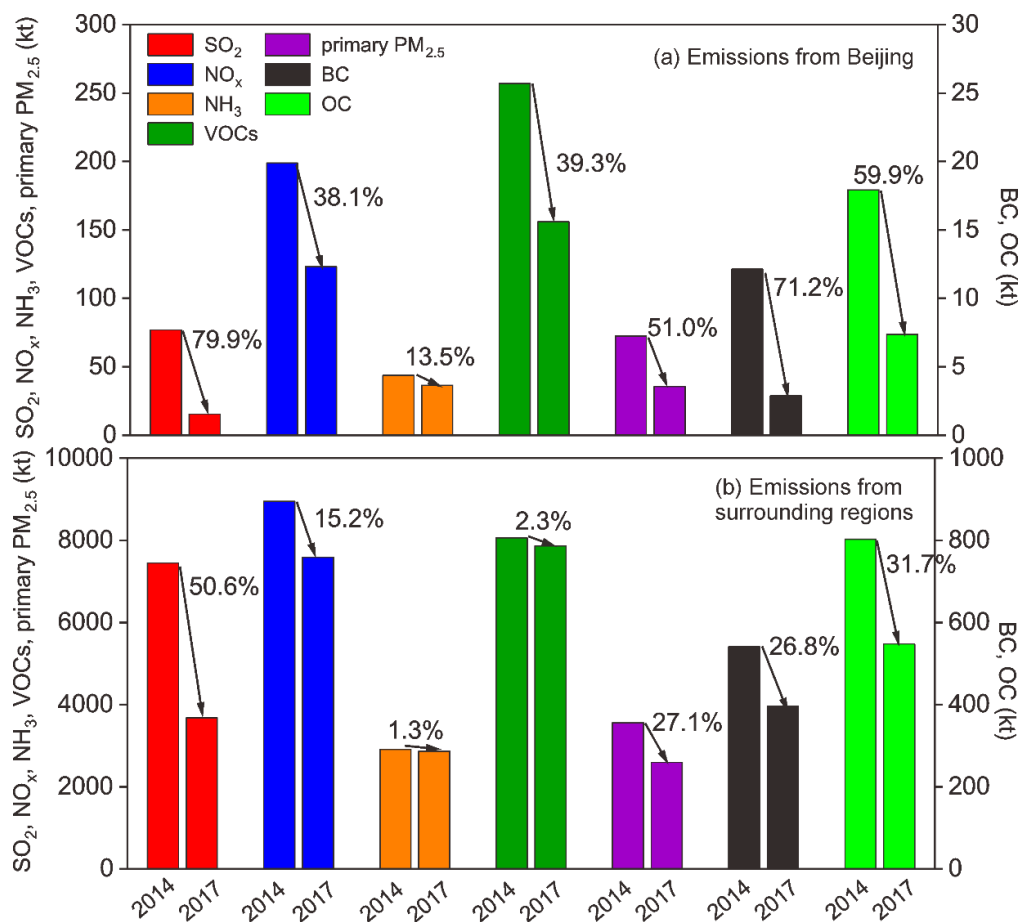
579

580 **Figure 4.** The average PM_{2.5} chemical composition simulated by the WRF-CMAQ model for the observation periods in 2017: (a) base
581 scenario with the 2017 emissions and the 2017 meteorological conditions; (b) simulation with the 2017 emissions and 2014 meteorological
582 conditions.



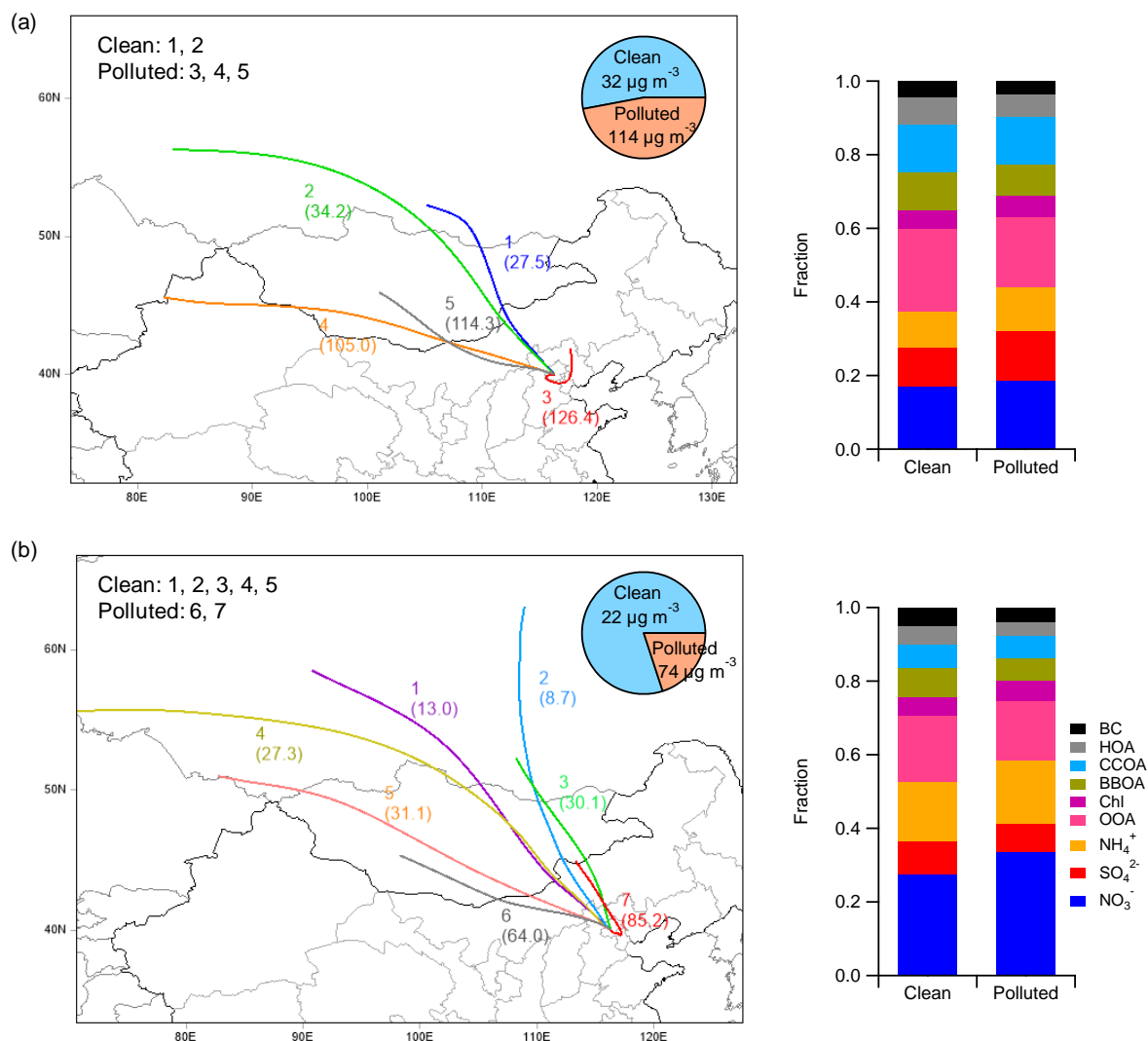
583

584 Figure 5. Simulated concentrations of $PM_{2.5}$ and its chemical components during the observation periods of 2014 and 2017: (a) total
585 changes in Beijing and (b) changes due to regional transport.

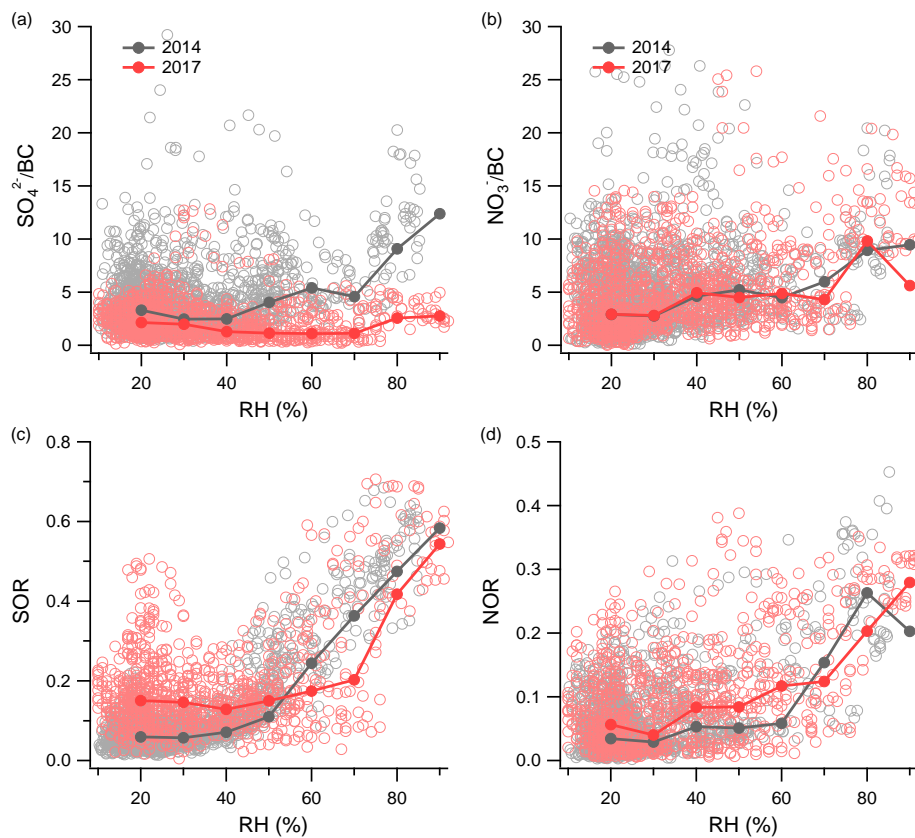


586

587 **Figure 6.** Changes in the anthropogenic emissions of SO₂, NO_x, NH₃, VOCs, primary PM_{2.5}, BC, and OC in (a) Beijing and (b) its
 588 surrounding regions from 2014 to 2017.

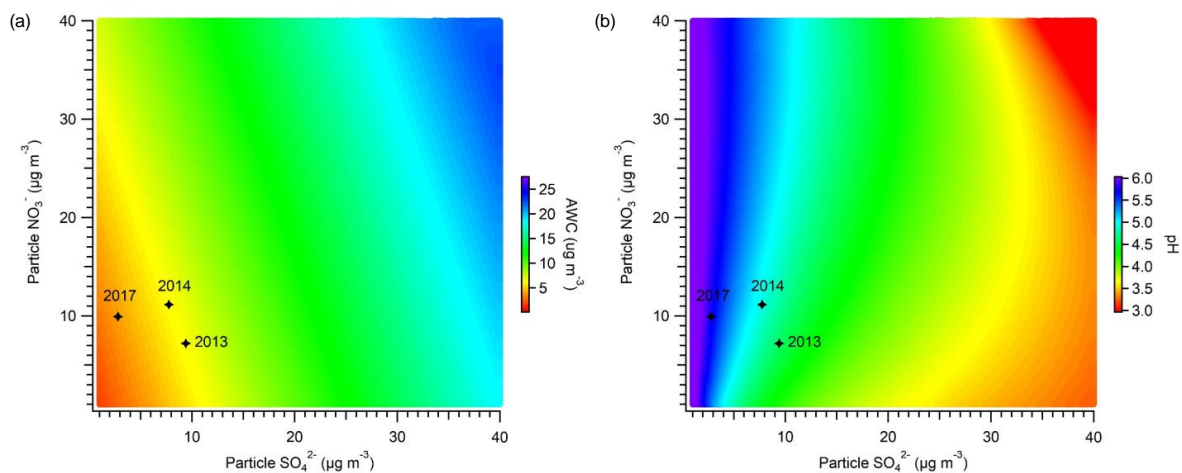


589
 590 **Figure 7.** Comparison of the air masses arriving in Beijing during the winters of 2014 and 2017. (a) and (b) show the clustering analysis of the back
 591 trajectories in the winters of 2014 and 2017, respectively, with pie charts displaying the contributions of the clean and polluted air masses.
 592 The stacked bar charts on the right show the average aerosol compositions for the clean and polluted clusters.



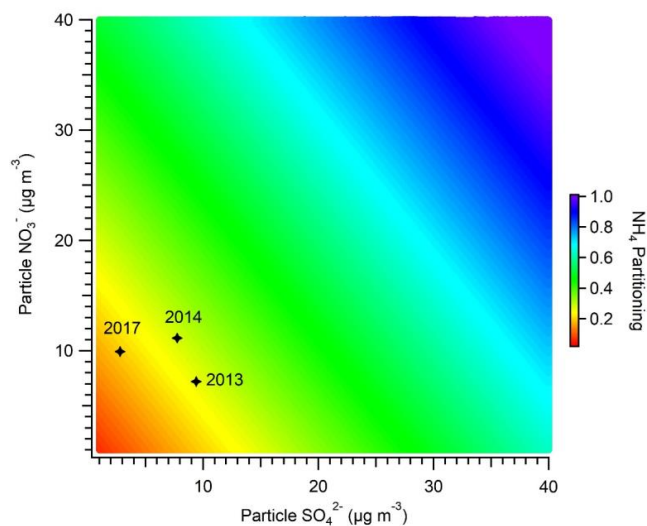
593

594 **Figure 8.** Variations in (a) SO_4/BC , (b) NO_3/BC , (c) SOR, and (d) NOR plotted against increasing RH. The data are also binned according
595 to RH values, with the median value shown for each bin.



596

597 **Figure 9. Sensitivity of (a) AWC and (b) particle pH to the mass concentrations of particulate sulfate and nitrate. The stars indicate the**
598 **average winter conditions for the years 2013, 2014, and 2017.**



599

600 **Figure 10.** Sensitivity of the ammonium partitioning ratio to the mass concentrations of particulate sulfate and nitrate. The stars indicate
601 the average winter conditions for the years 2013, 2014, and 2017.